Available online at www.sciencedirect.com
SCIENCE DIRECT
Polymer 47 (2006) 1141–1149
polymer
www.elsevier.com/locate/polymer

Influence of catalyst type on the curing process and network structure of alkyd coatings

S.J.F. Erich [a], J. Laven [a], L. Pel [a,*], H.P. Huinink [a], K. Kopinga [a]

[a] Department of Applied Physics, Eindhoven University of Technology, P.O. Box 513, 5600 MB Eindhoven, The Netherlands

Received 24 October 2005; received in revised form 19 December 2005; accepted 22 December 2005

Abstract

Recent studies have shown that cobalt catalysts, used for curing of alkyd coatings, are potentially carcinogenic, and hence replacement by new environmental friendly catalysts is needed. The influence of different metal based catalysts on the oxidation process has been studied extensively in model systems, consisting of unsaturated oils. However, these results may not be representative for real coatings, since in these systems the oxygen diffusion is much lower than in model systems and therefore may have a large effect on the curing. In this paper, we will show how the curing of an alkyd coating depends on the type of catalyst (cobalt or manganese based). The curing process is studied using a high spatial resolution nuclear magnetic resonance (NMR) setup. The final network structure and cross-link density are found to be correlated with the catalyst used, i.e. a cobalt based catalyst and two manganese based catalysts. The difference in final network structure is investigated by NMR T_2 relaxation analysis and the glass transition temperature T_g measured using a differential scanning calorimeter (DSC). In case of the cobalt based catalyst a cross-linking front was observed and a high cross-link density was found, compared to the manganese based catalysts, in which case no sharp cross-linking front was observed. To interpret the observed NMR profiles in more detail, simulations based on a reaction-diffusion model were performed. From the results of these simulations estimates were obtained for the reaction constants and the diffusion of oxygen for the different catalysts.

Keywords: Alkyd; Curing; NMR

1. Introduction

In the past 20 years, the concerns regarding the effect of chemicals on the environment have increased considerably. Recent studies have shown that cobalt, commonly used as a catalyst in alkyd coatings, is potentially carcinogenic [1–3]. Hence there is a tendency to replace this traditional catalyst by more environmental friendly ones in the near future. However, a change of catalyst in an alkyd coating has an impact not only on the chemical reactions taking place, but also on the curing behavior and the final network structure, as we will show in this paper. In order to find suitable alternatives the precise effects of the catalyst on the curing process have to be understood.

The research on curing of alkyd focusses on three aspects. First, the autoxidation processes of unsaturated fatty acids is studied in model systems [4–7]. Autoxidation is a very slow process in which various chemical species are formed while reacting with oxygen. The model systems that are investigated are usually oils, which remain liquid even after oxidation. The second area of interest deals with the influence of different catalysts, e.g. cobalt (Co) or manganese (Mn) based catalysts, on the oxidation process of these model systems [8–13]. The catalyst accelerates the formation of hydroperoxides and their decomposition into radical species. The cross-linking is driven by the reaction of these radicals. These investigations have led to valuable information concerning the chemical processes. The third area of interest deals with real alkyd coatings. In coating films an additional problem arises, which is the diffusion of oxygen. In contrast to model systems, in which the diffusion of oxygen is high because of the low viscosity and, therefore, does not affect the curing, the curing process of a coating film is influenced by the oxygen diffusion. The oxygen diffusion may limit the curing process of the coating and as a result it may influence the curing time and even the final

* Corresponding author.
E-mail address: l.pel@tue.nl (L. Pel).
http://www.phys.tue.nl/nfcmr/cmrmain.html.

0032-3861/$ - see front matter © 2006 Published by Elsevier Ltd.
doi:10.1016/j.polymer.2005.12.081

hardness. The actual curing process in a coating is the topic of this paper. This topic is of interest for coating manufacturers, because it directly links changes on molecular scale to the final coating and, consequently, to the product performance.

Recently, various techniques have become available to follow the curing process of a coating film in time with a high spatial resolution. One of these techniques is confocal Raman microscopy (CRM) in which the chemical changes can be probed locally, e.g. the change in double bonds [14–16]. Further, a nuclear magnetic resonance (NMR) setup has been developed with the ability to perform non invasive depth profiling of non-transparent coating systems, with a resolution of 5 μm [17]. This technique measures the density and mobility of the hydrogen nuclei, which can be obtained from the signal intensity and signal decay, respectively. The mobility of the polymers, and hence the mobility of the hydrogen atoms, decreases when polymers cross-link and form a network.

These two techniques allow the film formation process of alkyd coatings to be studied in more detail. This film formation or drying process can be divided into two stages. The first stage is a physical drying stage in which the solvent evaporates. This stage was studied extensively with high spatial resolution NMR [18–20]. The second stage is a curing (chemical drying) stage, in which the double bonds of the alkyd molecules vanish and cross-linking occurs. Using a high spatial resolution NMR setup the curing was studied by Mallegol et al. [10] for different drier combinations. As a primary drier (catalyst) cobalt was used, and as secondary driers Ca and Zr were used. They analyzed the curing process using the signal decay measured at three different positions inside the coating. In a previous paper, NMR and CRM results were used to interpret the relation between the NMR data and the chemical processes [21]. This study showed that the front observed because of the reaction of double bonds is directly related to the formation of cross-links. These experiments showed that NMR can be used to follow the cross-linking in non-transparent alkyd coatings. In a later study, the observed curing fronts were explained by a model that assumes that the curing process is limited by the oxygen diffusion towards the front [22].

In this paper, we will address the influence of two different manganese (Mn) and one cobalt (Co) based catalyst on the film formation process and the final network structure. First, the experimental details will be outlined in Section 2. Next, the results of the NMR measurements will be presented and discussed in Section 3. In Section 4, the data will be explained in more detail in terms of a reaction-diffusion model, and also the final network structure is discussed. Finally, the paper is concluded with a discussion in Section 5.

2. Experimental details

2.1. Materials

The measurements were performed on a water-borne alkyd emulsion with different catalysts. The alkyd emulsion used was made by DSM Coating Resins, Zwolle, The Netherlands [23]. The resin was synthesized based on soybean (50% regular; 50% conjugated) and phtalic acid. The curing was accelerated by the addition of a catalyst (either Nuodex WebCo 8%, Nuodex WebMn 9%, or MnMeTACN) to the emulsion (50% water and 50% oil) prior to film-casting. MnMeTACN is a diatomic manganese-based catalyst that is a potential alternative for cobalt containing catalysts. It has been reported that MnMeTACN acts as a highly effective catalyst during the oxidation of alkyd molecules [13,24]. The samples were cast on a 100 μm thick microscope cover glass. A spiral bar was used to cast a wet film with a thickness of about 200 μm. After application, the coating was directly placed in the NMR setup.

2.2. NMR setup

Magnetic resonance imaging (MRI) is a well known NMR technique for making images of the human body. Its principle is based on the fact that magnetic nuclei located in a magnetic field have a specific resonance frequency, and can be excited by a radio frequency (RF) pulse. The resonance frequency f depends linearly on the magnitude of the applied magnetic field $\vec{B}$, $f = \gamma|\vec{B}|$, with γ the gyromagnetic ratio (for hydrogen nuclei, $\gamma = 42.58$ MHz/T). To obtain one-dimensional (1D) profiles perpendicular to the film plane, the magnetic field should only vary with position in the y-direction, $B = B_0 + G_y y$, where $G_y = \partial B_z/\partial y$ denotes the field gradient in the y-direction and B_0, the magnetic field in the z-direction at $y = 0$. To obtain a high spatial resolution (< 10 μm) a very high magnetic field gradient should be applied. However, Maxwell's equations show that when a magnetic field gradient in a certain direction is applied, the magnitude of the field $|\vec{B}|$ in a plane perpendicular to that direction is not constant. At high field gradients the curvature of the surfaces with constant $|\vec{B}|$ becomes comparable to the measured sample volume. As a result the resonance frequency varies substantially within a horizontal plane inside the coating, resulting in a decrease of the effective 1D resolution.

To solve this problem, the so called GARField was introduced [17]. In this design a gradient in the magnitude of magnetic field was realized, $G_y^{\mathrm{mag}} = \mathrm{d}|\vec{B}|/\mathrm{d}y$ (Fig. 1) by creating special-shaped magnetic pole tips. It is then possible to distinguish thin layers within a film, that is oriented perpendicular to the y-direction. The advantage of a setup as shown in Fig. 1 is that a sample can be placed directly on top of a surface coil, which gives a good signal to noise ratio.

In our study, we use an NMR setup that contains an electromagnet generating a magnetic field of 1.4 T at the position of the sample. The field gradient is 36.4 ± 0.2 T/m.

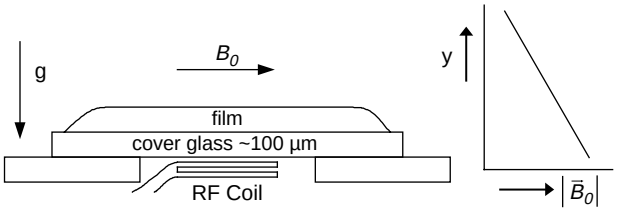

Fig. 1. RF coil and film placement in a high magnetic field gradient.

2.3. Interpreting the NMR signal decay

The NMR pulse sequence used to obtain the hydrogen density profiles and the signal decay is an Ostroff–Waugh (OW) [25] sequence ($90^{\circ}_{x} - \tau - [90^{\circ}_{y} - \tau - \text{echo} - \tau]_n$). The inter-echo time ($t_e = 2\tau$) used in the experiments equals 50, 100, or 200 μs. The theoretical spatial resolution increases when the duration of the signal recording window ($t_{rec} < t_e$) and hence the inter-echo time are increased, according to $\Delta y = 1/\gamma G t_{rec}$. The best achievable spatial resolutions corresponding to the inter-echo time settings given above are 13, 6.6, or 3.3 μm, respectively. The acquisition of each profile took about 10 min, using 512 signal averages.

The obtained NMR signals (S) give not only information on the density of the magnetic nuclei (in this case hydrogen nuclei) ρ, but also on the mobility of these nuclei. The network structure determines the mobility of the polymer chains, which is reflected by the transverse relaxation time T_2, describing the decay of the NMR signal. In general this signal decay can be described by

$$S(mt_e) = \sum_i S_i \exp\left(\frac{-mt_e}{T_2^i}\right) \quad (1)$$

where t_e denotes the inter-echo time and m the sequence number of the acquired echo, and a sum over all T_2 values is observed. The mobility of the hydrogen nuclei may vary within the coating and therefore different T_2 values can be observed at different positions. The cross-links have a low mobility (short T_2) and the polymer chains between the cross-links have a high mobility (long T_2) [26–28]. Note that with this NMR setup the signal intensity and the signal decay are obtained as a function of depth within the coating.

After curing of the alkyd resin, the mobility of the polymer has decreased significantly because of the cross-linking, which results in a fast signal decay, governed by the interaction between the rigid nuclear dipoles [29]. However, when the signal decay is measured with the OW sequence, at small inter-echo time settings a slightly increased effective T_2 is observed [30]. Therefore, T_2 values can only be compared at fixed inter-echo time settings. In Fig. 2, the signal decay of a completely cured alkyd resin is depicted. The duration of the recording window and, consequently, the inter-echo time should be carefully chosen. When the characteristic T_2 time governing the signal decay is much shorter than the inter-echo time, the resolution is not only determined by the time of the recording window, but also by the T_2-value. In such a case, the duration of the recording window (and hence the inter-echo time t_e) should be decreased, so that more points are measured in a typical decay curve. This makes discrimination of different short relaxation times possible. This is illustrated by the dashed line in Fig. 2, which is a fit for the echo decay observed when using $t_e = 100$ μs as inter-echo time setting. For the setting $t_e = 50$ μs one can see that more relaxation times can be distinguished. Note that the first data point is located significantly above the dashed line. An increase of the duration of the recording window also results in a decrease of the SNR,

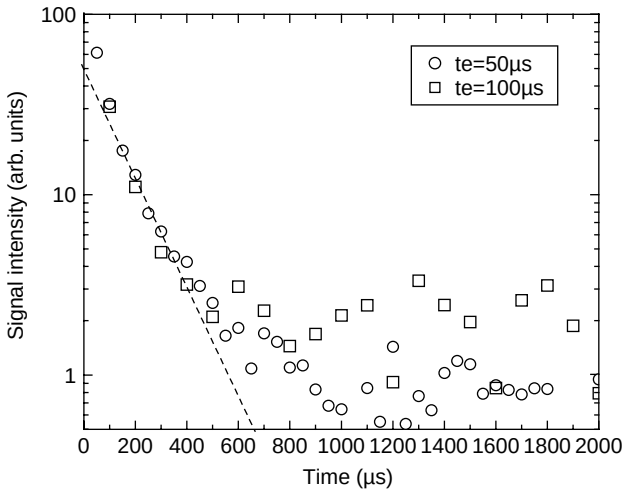

Fig. 2. Typical signal decay of a cured alkyd resin, measured using an Ostroff–Waugh sequence. By increasing the inter-echo time from 50 to 100 μs the fast signal decay below 100 μs is missed. Also the signal to noise ratio (SNR) decreases, which is a consequence of the increased spatial resolution. The dashed line is a fit to the echo decay observed when using $t_e = 100$ μs as inter-echo time setting.

caused by a decrease of the 1D voxel size. These three effects, the missing of fast relaxation times, the decrease of the SNR, and a shorter effective T_2 at longer inter-echo times, cause that in this film no signal is observed from the cross-linked areas at an inter-echo time $t_e = 200$ μs.

2.4. Differential scanning calorimeter

Glass transition temperatures of the coatings were determined using a Mettler Toledo differential scanning calorimeter 822^e. The experiments were started at −50 °C and next the sample was heated up to 80 °C, with a ramp speed of 10 °C/min using a 20 μl aluminum crucible. The glass transition temperature was determined from the second run, to eliminate the 'memory' (the thermal history of the system) effects seen in the first run [31].

3. Results

3.1. Curing process

The influence of the catalyst on the curing process was investigated by analyzing the observed changes in the acquired NMR profiles. The profiles obtained from measurements on the water-borne alkyd coating using a 0.07% m/m concentration of cobalt catalyst are shown in Fig. 3.

NMR measurements were performed with two different inter-echo time settings, $t_e = 100$ and 200 μs, shown in Fig. 3(a) and (b), respectively. At the right side of these profiles the cover glass is positioned. The slope of the profiles at the coating/glass interface is limited by the experimental resolution. At the left side the surface of the coating is located, which is in contact with the surrounding air. The profiles are acquired every 10 min; only a subset of the profiles is represented in the figure after interpolation over all acquired

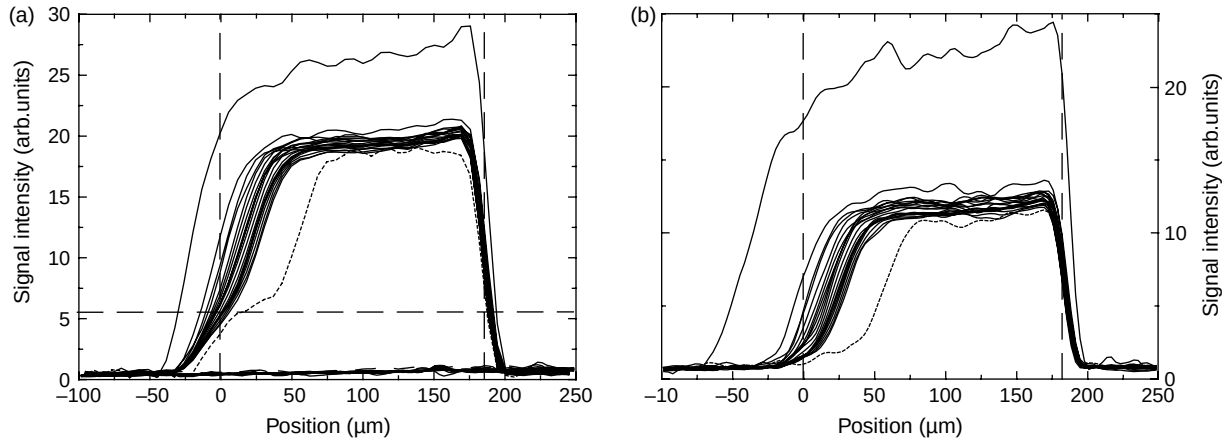

Fig. 3. NMR profiles for 0.07% Co metal mass to the mass of the alkyd resin. The profiles were acquired using an inter-echo time setting (a) $t_e = 100$ μs (b) $t_e = 200$ μs. The profiles are given every 9.6 h. The dashed profile is measured after 21 days of curing. The left vertical dashed line indicates the top of the coating after evaporation. The right vertical dashed line indicates the bottom of the coating on top a cover glass. The horizontal dashed line in figure a shows the signal remaining after the complete curing process.

profiles. First, we observe a drying stage in which water evaporates from the emulsified alkyd. During this stage the height of the profiles decreases and some shrinkage of the film occurs at the left side of the profiles. The first profile plotted in Fig. 3 is measured just after application of the film. After about 5 h of drying, between the first and second profile shown in Fig. 3, a front develops, which moves towards the bottom of the coating. Above this front a glassy skin layer has formed, and underneath this layer uncross-linked resin remains. In Fig. 3(a) a plateau corresponding to a signal level of about 5 a.u. starts to form, which is the signal that remains after cross-linking has occurred. This is most clearly visible in the profile obtained after 21 days of curing given by the dashed curve. The front becomes visible because of a decrease of the relaxation time when cross-linking occurs, as was discussed in Section 2.3. In Fig. 3(b), in which the signal is acquired 200 μs after excitation, the signal of the cross-linked part has vanished completely, and the difference between the cross-linked and uncross-linked region is more pronounced. However, since the cross-linked region is no longer visible, the movement of the left edge of the profile could erroneously be interpreted as shrinkage of the film. Therefore, only the profiles acquired with an inter-echo time setting of $t_e = 100$ μs will be shown from now on.

The results of similar measurements on a sample with WebMn and MnMeTACN as a catalyst are plotted Fig. 4(a) and (b), respectively. A curing front is still present in these profiles, but it is not as sharp as is the case for cobalt (Fig. 3). These samples cure more homogeneously, indicating that oxygen penetrates the coating much further than for the cobalt catalyst. The final stage of the curing process, in which no changes are observed anymore, is reached in about one week for the Mn based catalyst, which is much faster than for the Co based catalyst. In case of Co, the observed sharp front takes several months to reach the bottom of the coating. In both Fig. 4(a) and (b), one can clearly see that relative signal decrease during curing is much smaller than for the sample with WebCo as a catalyst. This indicates that the polymers remain more mobile and the network has a lower cross-link density. In Section 3.2, we will further discuss the correlation between the curing behavior and the final network structure that is formed.

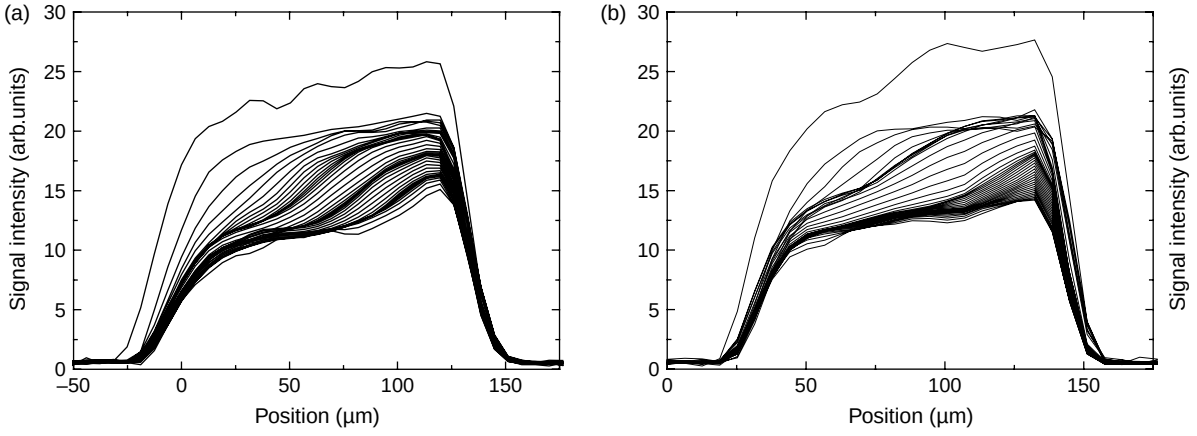

Fig. 4. NMR profiles for 0.07% Mn metal mass to the mass of the alkyd resin. (a) Cured with WebMn catalyst, profiles are given every 7.8 h. (b) Cured with MnMeTACN catalyst, profiles are given every 3.5 h. The profiles were acquired using an inter-echo time setting $t_e = 100$ μs.

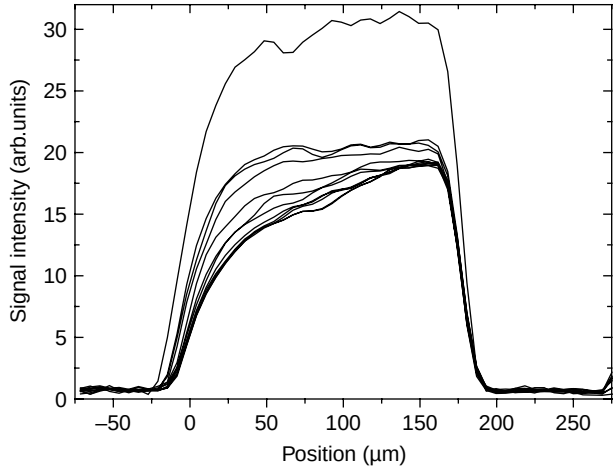

Fig. 5. NMR profiles for 0.0007% Co metal mass to the mass of the alkyd resin. The profiles are given at $t=0$; 10.4 h, and then every 13 h. The profiles were acquired using an inter-echo time setting $t_e=100$ μs.

To check whether the change in behavior for the manganese based catalyst is only a matter of change in reaction rate, the normally used Co based catalyst concentration was diluted by a factor of 100. In Fig. 5 the NMR profiles for this sample are shown. In this case, no sharp curing front is present and the results resembles those of the Mn based catalyst. We will further discuss this result in Section 4.

3.2. Final network structure

Confocal Raman microscopy can be used to obtain spatially resolved chemical information inside a transparent coating film [14–16,22,32]. The samples measured by NMR were also analyzed using CRM after 6 months of curing to see whether double bonds have remained. This enable us to check whether the cross-link density in the samples with the Mn based catalysts is indeed less dense, as suggested by the NMR measurements. In Fig. 6 the results of these CRM measurements are shown. Because at every position inside the coating the same behavior was observed, only the average is shown.

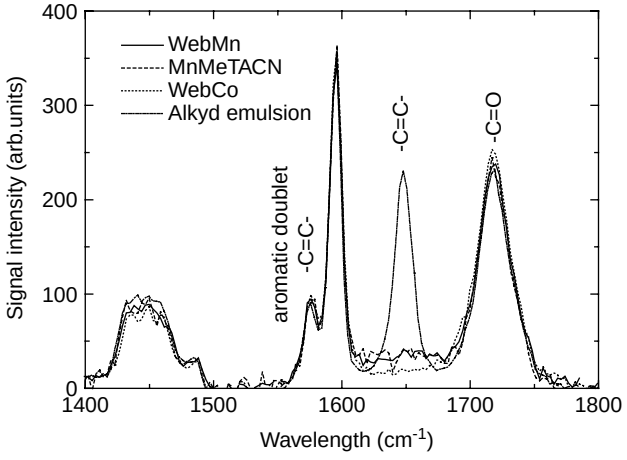

Fig. 6. Results obtained using confocal Raman microscopy for the three catalyst used. No double bonds remain after complete curing of the coating.

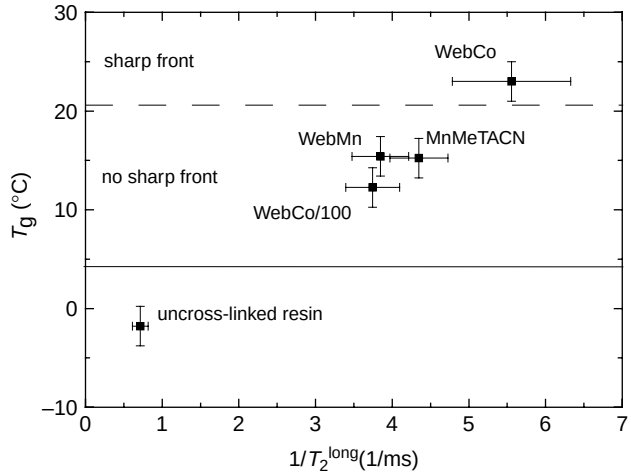

Fig. 7. Relation between T_2 measured with NMR and T_g measured with a DSC.

The double bonds (at 1650 cm^{-1}) that are present before curing are clearly visible, but after about 6 months this signal has completely vanished for all types of catalyst. Also T_2 measurements on these samples were performed to measure the mobility. After cross-linking the T_2 values are very short. Therefore, the NMR signal decay was measured using an inter-echo time of 50 μs, at the cost of spatial resolution. Using this setting bi-exponential behavior of the signal decay was observed. Only the longest relaxation time T_2^l contributing to this decay was used in the analysis. Also DSC measurements were performed to obtain the glass-transition temperature (T_g) of these samples. The value of T_g found for the different catalysts, catalyst concentrations, and for the uncross-linked alkyd resin is plotted against T_2^l in Fig. 7. This figure reveals a distinct correlation between T_2^l and T_g. The results also show that if a front is visible during the curing process, a high T_g is observed and T_2^l is short. When no sharp front was visible (all cases except for the normal concentration of cobalt catalyst) T_g was significantly lower and T_2^l longer.

We conclude that even though CRM shows complete curing, NMR and DSC still show differences in the final network structure as a result of changes in catalyst or catalyst concentration, which indicates that changes have occurred during the curing of the alkyd resin.

4. Model

To explain the observed characteristics in more detail we need to obtain information on the reaction rate and the diffusion of oxygen for the different catalysts. To achieve this, the evolution of the NMR profiles of curing alkyd resins was described by a reaction-diffusion model and by the change of the signal decay caused by the cross-linking. In Section 4.1, the reaction-diffusion equations are discussed, and in Section 4.2, the NMR profiles are explained in more detail, using a model describing the change of the signal decay as a function of the degree of cross-linking. In Section 4.3, the predictions from the reaction-diffusion model are compared with the NMR results.

Table 1
Fixed initial values used in the numerical simulations. The values of S_i and T_2^i are chosen to correspond with the experimental values obtained from the NMR data

ρ_d^i (mol/m^3)	ρ_o^i (mol/m^3)	n (mol/mol)	S_s (a.u.)	T_2^s (μs)	S_l (a.u.)	T_2^l (μs)
2000	3	1.0	37	50	17	1000

4.1. Reaction-diffusion equations

The reaction of oxygen with fatty acid side chains of the alkyd resin causes a decrease of the concentration of double bonds ρ_d (mol/m^3) and the formation of cross-links. The oxygen diffusivity D (m^2/s) generally depends on the mobility of the polymers. The oxygen density ρ_o (mol/m^3) inside the coating is determined by oxygen diffusion as well as the reaction of oxygen with the double bonds and can be described by

$$\frac{\partial \rho_d}{\partial t} = -k\rho_o\rho_d \tag{2}$$

$$\frac{\partial \rho_o}{\partial t} = \frac{\partial}{\partial x}\left(D(\rho_d)\frac{\partial \rho_o}{\partial x}\right) - nk\rho_o\rho_d \tag{3}$$

in which k (m^3/mol s) denotes the reaction rate of the oxygen with the double bonds, and n (mol/mol) denotes the amount of oxygen reacting per double bond. We will assume $D(\rho_d)=D$ in all numerical calculations. The boundary conditions are specified as follows

$$\rho_o(0,t) = \rho_o^i \tag{4}$$

$$\frac{\partial \rho_o}{\partial x}(L,0) = 0 \tag{5}$$

$$\rho_o(x,0) = 0 \tag{6}$$

$$\rho_d(x,0) = \rho_d^i \tag{7}$$

where L is the coating thickness and denotes the position of the microscope glass. At $x=L$ the the oxygen flux is zero, whereas at the surface the oxygen density is equal the solubility density. The oxygen density within the film is taken equal to zero at the start of the curing process. The initial values are given in Table 1.

4.2. NMR profiles

The measured NMR signal decay of the alkyd coatings is governed by multiple relaxation times (Eq. (1) and Section 2.3) when the resin is not cross-linked. If an inter-echo time $t_e=100$ μs is used, two relaxation times are observed before cross-linking. After cross-linking only one relaxation time can be observed, see also [21]. Therefore, the signal decay can be described by

$$S(mt_e) = S_s(t)\exp\left(\frac{-mt_e}{T_2^s}\right) + S_l(t)\exp\left(\frac{-mt_e}{T_2^l}\right) \tag{8}$$

where $S(mt_e)$ is the NMR signal during the NMR experiment and m the sequence number of the echo. Note that mt_e is of the order of ms, whereas the time t corresponds to the time scale of the curing process, which is of the order of hours or days. S_s is the intensity of the signal corresponding to the short relaxation time T_2^s and S_l the intensity of the signal corresponding to the long relaxation time T_2^l. In all numerical simulations average values for T_2^l and T_2^s were taken, although, for the manganese based catalyst slightly higher values of T_2^s were observed.

We assume that when the cross-linking occurs the mobile chains become immobile, so the contribution of S_l to the observed NMR signal will be incorporated in S_s. This signal change is assumed to be proportional to the amount of double bonds present. This automatically implies that when no double bonds are present any more only one relaxation time is observed, which agrees with the results of our NMR measurements.

Additionally, the simulated profiles are convoluted with the observed experimental resolution of about 10 μm to enable a more direct comparison between simulations and measurements.

4.3. Results

Combining the reaction diffusion equation and the equations relating the NMR signal profiles to the cross-linking process, numerical simulations can be performed. We have performed calculations on four different systems that represent the ones presented in Section 3.1. For these four coatings the fixed parameters have to be specified. We need the amount of double bonds ρ_d, oxygen concentration ρ_o, amount of oxygen per double bond n, diffusion constant D, and reaction constant k. The values of S_s, S_l, T_2^s and T_2^l were determined from the NMR data. Table 1 shows the initial values that are taken constant in all numerical simulations. The only parameters that are varied are the diffusion and reaction constant. The alkyd used has an oil length of 40, which corresponds to 400 kg/m^3. Taking a molar mass of about 300 g/mol for the fatty acid chain gives 1200 mol/m^3 of oil chains. Since each oil chain contains on average two double bonds ρ_d is set at 2×10^3 mol/m^3. From oxygen uptake measurements of ethyllinoleate, a model system, it is known that n, the amount of oxygen molecules per double bond, is about 0.75 in case of a manganese based

Table 2
Values for the diffusion constant, reaction constant, and layer thickness used in the different simulations. The figures displaying the simulated results are also indicated

Catalyst	D (m^2/s)	k (m^3/mol s)	L (μm)	Figure
WebCo	10^{-12}	1×10^{-4}	200	8
WebCo/100	4×10^{-12}	1×10^{-6}	200	9
WebMn	8×10^{-12}	5×10^{-6}	150	10
MnMeTACN	2×10^{-11}	5×10^{-6}	125	11

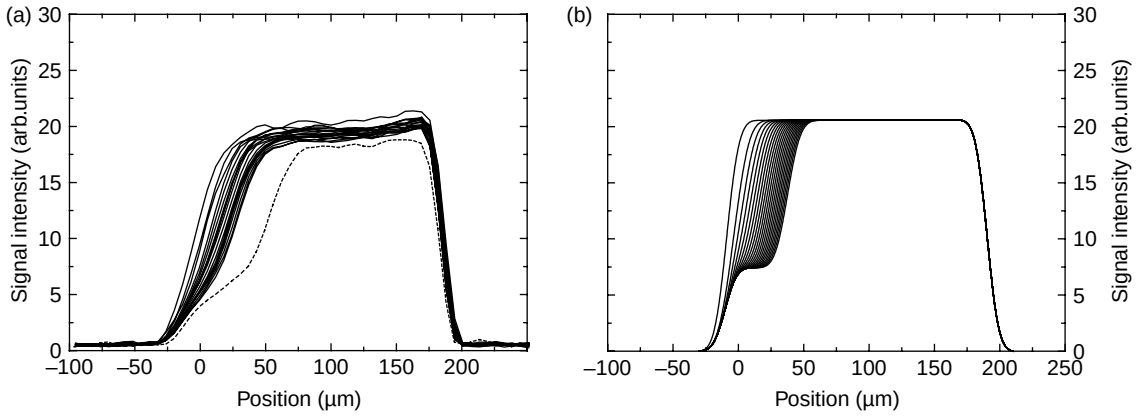

Fig. 8. Time and position dependence of the NMR hydrogen signal for the WebCo catalyst (a) experimental data (b) results obtained from a reaction–diffusion–relaxation NMR model. $D=10^{-12}$ m^2/s, $k=1\times10^{-4}$ m^3/mol s, $L=200$ μm. In the the left graph the dotted profile after 21 days of curing is plotted to make the formation of the plateau more clearly visible.

catalyst and about 1.1 in case of a cobalt based catalyst [13,24], so n will be taken equal to 1. The oxygen solubility in oil is estimated as 3 mol/m^3 [23,32,33].

For the four different coating systems simulations were performed, at time intervals similar to the measured profiles. Note that the evaporation stage is not included in the simulations. The thickness of the coating in the simulation was set to the thickness measured using the NMR setup. For the different catalysts the values for the diffusion and reaction constant used in the simulations are given in Table 2. They were chosen such that a good match between the simulations and the observed profiles was obtained. Although these values should only be considered as crude estimates, due to the inaccuracy in the initial values given in Table 1, they can be used to explain the observed tendencies of the curing behavior. The results for the film containing WebCo as a catalyst are plotted in Fig. 8. The simulated results clearly show the cross-linking front moving to the right that is present in the experimental data. Clearly, oxygen diffusion is the limiting step, see also the high reaction constant and low diffusion constant in Table 2. Since, in the cross-linked region the T_2 is very short, the actual experimental resolution is lower than that was used in the simulations. This explains why, in contrast to the simulations, the plateau observed in the measurements after 21 days of curing is not horizontal. For the diluted WebCo (Fig. 9) the reaction constant in the simulation was decreased by a factor of 100, equal to the dilution of the catalyst, which implicitly assumes that the reaction constant is proportional to the catalyst concentration. An increase of the diffusion constant was needed to obtain a behavior matching the results of the NMR measurements, which is reasonable if the coating is less densely cross-linked. For the WebMn and MnMeTACN catalysts the reaction constant was kept constant at 5×10^{-6} m^3/mol s, whereas the diffusion constant was varied to obtain a good match with the experimental data, see Figs. 10 and 11. The diffusion constant ranges between 10^{-11} and 10^{-12} m^2/s, which is within the range of values reported in the literature [34,35]. The reaction constants correspond fairly well to representative reaction constants given in the literature [36].

If we compare the simulations of the NMR profiles with the NMR measurements for the manganese based catalysts, we observe that the signal intensity that remains in the NMR

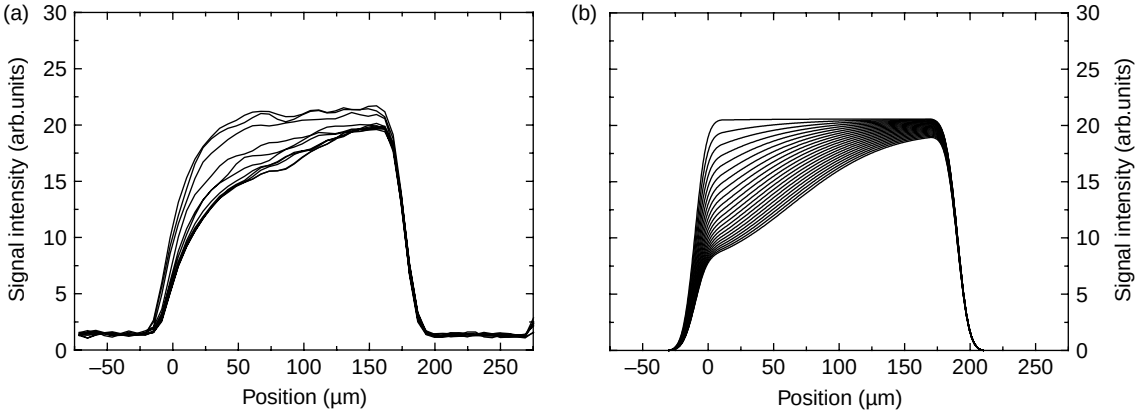

Fig. 9. Time and position dependence of the NMR hydrogen signal for the 100 times diluted WebCo catalyst (a) experimental data (b) results obtained from a reaction–diffusion–relaxation NMR model. $D=4\times10^{-12}$ m^2/s, $k=1\times10^{-6}$ m^3/mol s, $L=200$ μm.

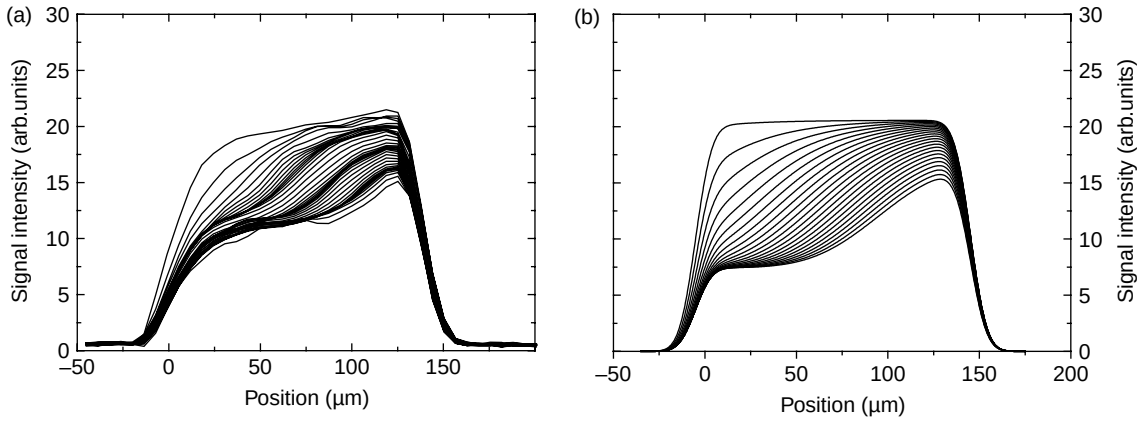

Fig. 10. Time and position dependence of the NMR hydrogen signal for the WebMn catalyst (a) experimental data (b) results obtained from a reaction–diffusion–relaxation NMR model. $D=8\times10^{-12}$ m^2/s, $k=5\times10^{-6}$ m^3/mol s, $L=125$ μm.

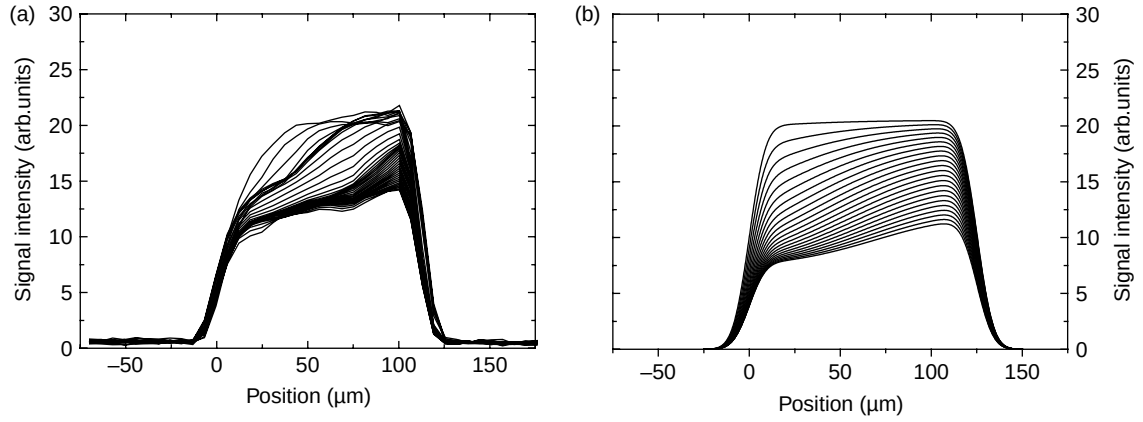

Fig. 11. Time and position dependence of the NMR hydrogen signal for the MnMeTACN catalyst (a) experimental data (b) results obtained from a reaction–diffusion–relaxation NMR model. $D=2\times10^{-11}$ m^2/s, $k=5\times10^{-6}$ m^3/mol s, $L=150$ μm.

measurements in the cross-linked region is larger than the signal intensity in the simulations. This is caused by the fact that the value of T_2^s in these systems is somewhat larger than the average value used or the simulations. The CRM measurements have indicated that all double bonds have reacted, but the results from the NMR T_2 and the T_g measurements plotted in Fig. 7 indicate a higher polymer mobility. The final network structure seems to be less dense than for the WebCo catalyst, which explains the higher diffusion coefficient needed as input for the simulation of the NMR profiles. A possible explanation of this change in network structure may be a change of reaction routes of the oxidation mechanism of unsaturated fatty acids, but this is beyond the scope of this paper.

For the coating with the WebCo catalyst, shown in Fig. 8, the reaction constant is the highest and the diffusion constant used in the simulation is the lowest. The high reaction rate is the bases for the formation of a glassy skin. In this glassy skin the polymer mobility is very low, because it is fully cross-linked, making diffusion of oxygen difficult. For the other catalysts the cross-linking process is not complete, and diffusion takes place through a partly cross-linked region. Since the diffusion constant is expected to decrease during curing, the diffusion varies as function of position inside the coating. Based on the diffusion constants given in Table 2, we estimate that the diffusion varies at most within one order of magnitude. Because in the simulations the diffusion is assumed to be constant, the results at long simulations times may differ from the experimental data.

5. Conclusions

Using NMR depth profiling we observed distinct changes in curing behavior for different catalysts. For a cobalt based catalyst a sharp drying front was observed, whereas for the manganese based catalysts no sharp front was observed. Additionally, the final network structure after complete curing was analyzed by DSC and NMR. A decrease in glass transition temperature T_g for the manganese catalysts compared to the cobalt catalyst was found. Also a clear correlation between T_g and the NMR relaxation time T_2 was found; with increasing T_g the value of T_2 decreases. When a sharp cross-linking front was present in the NMR data, the final cross-link density was found to be higher, indicated by both the T_2 and T_g values. This behavior might be explained by changes in the complex autoxidation mechanisms involved in the cross-linking of alkyd resins [4,5,7,37], which is beyond the scope of this paper.

The differences in curing speed observed for the WebCo, WebMn, and MnMeTACN catalyst can be explained by changes in reaction rate and oxygen diffusion constant only. A change of the diffusion constant seems to be necessary to obtain a good match between the simulations and the experimental NMR profiles. An increase of the diffusion coefficient indicates that the network structure is less rigid, which is corroborated by the lower cross-link density found for the low concentration of WebCo and for the manganese based catalysts.

Replacing the cobalt based catalyst in coatings obviously results in completely different curing behavior, whereas also the final hardness seems to change. Our study unambiguously demonstrates that the consequences of replacement of the catalyst cannot solely be assessed from measurements on model systems, but also knowledge on the curing behavior inside a coating is required. High resolution nuclear magnetic resonance has proven to be an excellent tool to achieve a more in-depth knowledge of the curing behavior and degree of cross-linking in coatings.

Acknowledgements

This research was supported by the Center for Building and Systems TNO-TUE.

References

[1] Lison D, de Boeck M, Verougstraete V, Kirsch-Volders M. Occup Environ Med 2001;58:619–25.
[2] Bucher JR, Hailey JR, Roycroft JR, Haseman JK, Sills RC, Grumbein SL, et al. Toxicol Sci 1999;49:56–67.
[3] de Boeck M, Kirsch-Volders M, Lison D. Mutat Res 2003;533:135–52.
[4] Porter NA, Lehman S, Weber BA, Smith KJ. J Am Chem Soc 1981;6447–55.
[5] Porter NA, Wujek DG. J Am Chem Soc 1984;2626–9.
[6] Hubert JC, Venderbosch RAM, Muizebelt WJ, Klaasen RP, Zabel KH. J Coat Technol 1997;69:59–64.
[7] Muizebelt WJ, Donkerbroek JJ, Nielen MWF, Hussem JB, Biemond MEF, Klaasen RP, et al. J Coat Technol 1998;70:83–93.
[8] Muizebelt WJ, Hubert JC, Nielen MWF, Klaasen RP, Zabel KH. Prog Org Coat 2000;40:121–30.
[9] Mallegol J, Lemaire J, Gardette JL. Prog Org Coat 2000;39:107–13.
[10] Mallegol J, Barry AM, Ciampi E, Glover PM, McDonald PJ, Keddie JL, et al. J Coat Technol 2002;74:113–24.
[11] Bieleman JH. Macromol Symp 2002;187:811–21.
[12] Oyman ZO, Ming W, van der Linde R. Prog Org Coat 2003;48: 80–91.
[13] Oyman ZO, Ming W, Micciche F, Oostveen E, van Haveren J, van der Linde R. Polymer 2004;45:7431–6.
[14] Schrof W, Beck E, Koniger R, Reich W, Schwalm R. Prog Org Coat 1999; 35:197–204.
[15] Schrof W, Beck E, Etzrodt G, Hintze-Bruning H, Meisenburg U, Schwalm R, et al. Prog Org Coat 2001;43:1–9.
[16] Froud CA, Hayward IP, Laven J. Appl Spectrosc 2003;57:1468–74.
[17] Glover PM, Aptaker PS, Bowler JR, Ciampi E, McDonald PJ. J Magn Reson 1999;139:90–7.
[18] Ciampi E, Goerke U, Keddie JL, McDonald PJ. Langmuir 2000;16: 1057–65.
[19] Gorce JP, Bovey D, McDonald PJ, Palasz P, Taylor D, Keddie JL. Eur Phys J, E 2002;8:421–9.
[20] Ciampi E, McDonald PJ. Macromolecules 2003;36:8398–405.
[21] Erich SJF, Laven J, Pel L, Huinink HP, Kopinga K. Appl Phys Lett 2005; 86:134105.
[22] Erich SJF, Laven J, Pel L, Huinink HP, Kopinga K. Prog Org Coat 2005; 52:210–6.
[23] Laven J, Uravind UK. The chemical drying process in alkyd emulsion paint films. Athens Conference on Coatings Science and Technology; 2003.
[24] Oyman ZO. Towards environmentally friendly catalysts for alkyd coatings. Thesis/Dissertation Thesis. Technische Universiteit Eindhoven; 2005.
[25] Ostroff ED, Waugh JS. Phys Rev Lett 1966;16:1097–8.
[26] Litvinov VM, Dias AA. Macromolecules 2001;34:4051–60.
[27] Gotlib YY. Polym Sci USSR 1975;17:1850.
[28] Gotlib YY. Polym Sci USSR 1976;18:2299–3003.
[29] Bloembergen N, Purcell EM, Pound RV. Phys Rev 1948;73:679–712.
[30] Mansfield P, Ware D. Phys Rev 1968;168:318–34.
[31] Hohne GWH, Hemminger WF, Flammersheim H-J. Differential scanning calorimetriy. 2nd ed. Heidelberg: Springer; 2003.
[32] Marton B. A depth-resolved look at the film formation and properties of alkyd-based coatings. Thesis/Dissertation Thesis. University of Twente; 2004.
[33] Landolt H, Boernstein R. 6th ed Zahlenwerte und Funktionen aus Physik, Chemie, Astronomie, Geophysik und Technik, vol. IV. Berlin: Springer; 1980.
[34] Hormats EI, Unterleitner FC. J Phys Chem 1965;69:3677–81.
[35] Audouin L, Langlois V, Verdu J, Debruijn JCM. J Mater Sci 1994;29: 569–83.
[36] Wallin M, Glover PM, Hellgren AC, Keddie JL, McDonald PJ. Macromolecules 2000;33:8443–52.
[37] Muizebelt WJ, Nielen MWF. J Mass Spectrom 1996;31:545–54.